New Physical Insight into High-Spin Physics: Double Helix Level Scheme

A nuclear structure data approach

Ninel Nica[1,*]

[1]Cyclotron Institute, Texas A&M University, College Station, Texas 77843, USA

Abstract. To present a new nuclear structure data concept of a level scheme, we redesign the high-spin level scheme of ^{171}Yb nucleus. We start with the description of the property of *repeatability* of the E_γ data based on which E_γ can be parametrized by the $2c(2I + k - 1)$ formula with I the nuclear spin and k an integer band offset different from band to band. This describes a beam of parallel and equidistant lines whose $2c$ average slope and k numbers can be determined by a least-squares fit to the experimental bands, which characterize the average rotational behavior of the experimental bands. Based on repeatability the level scheme of ^{171}Yb nucleus can be shaped as a discrete $3D$ double helix structure, with the experimental bands superimposed as decay paths. Double helix suggests that semiclassically nuclear rotation can be seen as a vortex motion.

1 Introduction

Level scheme is an old tool to schematically present nuclear structure data. Starting from the ground state the levels are ordered by their excitation energy, indexed by spin and parity, and interconnected by the decaying radiation. Here we deal only with level schemes composed of the typically long cascades of the γ-ray rotational bands in high-spin physics. They are primarily described by the basic model of Bohr and Mottelson [1] based on the $I(I + 1)$ parametrization and the underlaying nuclear rotation physics. Several other more sophisticated parameterizations were design to fit the experimental data as for example those in Refs. [2, 3].

In this paper we use a new phenomenological parametrization that we first introduced in [4], from which we deduced the new $3D$ concept of a *double helix* level scheme on which the experimental rotational bands can be superimposed. In that paper we described in detail the algorithmic method leading to the double helix concept for even-A and odd-A nuclei and applied it for illustration to the rotational bands of ^{171}Yb nucleus [5].

Following this introduction, in this paper we start in Section 2 with the two-fold experimental evidence that led to the double helix concept. Then, in Section 3 we review shortly the construction of the double helix level scheme of ^{171}Yb nucleus. Although a proper physical interpretation is not possible at this still preliminary stage, in Section 4 we try to foresee some of the new physical insight that double helix level scheme could bring to the high-spin physics. Finally, some concluding remarks are included.

*e-mail: nica@comp.tamu.edu

2 Experimental evidence

In this section we present the two facets of *repeatability*, the experimental evidence that lead to the new concept of double helix level scheme.

2.1 $(\Delta E_\gamma^x, \Delta E_\gamma^y)$ differential distributions

Bohr-Mottelson collective rotor gives the basic description of the rotational bands. Thus the E_{level} level energy as function of spin I and moment of inertia $\Im$ is given by:

$$E_{level}(I) = \frac{\hbar^2}{2\Im} I(I+1) = cI(I+1) \qquad (1)$$

where we denoted by c the inertial parameter, $c = \frac{\hbar^2}{2\Im}$. The γ-ray energy E_γ can be calculated from the difference of two consecutive levels:

$$E_\gamma(I) = E_{level}(I) - E_{level}(I-2) = 2c(2I-1) \qquad (2)$$

We can also define the $\Delta E_\gamma(I)$ quantity as the difference between two consecutive γ-ray energies:

$$\Delta E_\gamma(I) = E_\gamma(I) - E_\gamma(I-2) = 8c \qquad (3)$$

For an ideal rotor the moment of inertia is constant and the above spin dependencies are purely quadratic for eq. 1, purely linear for eq. 2 and a constant for eq. 3, while for real rotors there are deviations from the pure dependencies.

Eq. 3 says that the spectrum of the γ rays for the ideal rotor is formed of $8c$ equidistant lines. Now let us take all the set of coincidence points (E_γ^x, E_γ^y) of the ideal rotor band and get the $(\Delta E_\gamma^x, \Delta E_\gamma^y)$ differential distribution by taking the difference between any two coincidences of this set. For the ideal rotor band, we get a $2D$ regular grid

of equidistance of $8c$ on both axes, with statistics only at the crossings of the regular grid.

What happens if instead of the ideal rotor band we take the real experimental bands of ^{171}Yb nucleus from [5]? For the real bands the moment of inertia fluctuates, which produce deviations from the equidistant $8c$ grid. Or, according to the *Fluctuation Analysis Method* developed by B. Herskind ([6, 7] and references therein) these fluctuations are random.

As we neglected the intensity information of the coincidences, then the $(\Delta E_\gamma^x, \Delta E_\gamma^y)$ differential distribution is a bitmap distribution. On average we can still distinguish an equidistant grid characterized by the so called *effective second moment of inertia*, $\Im^{(2)}_{eff}$, but with the points spread randomly from its crossings.

In Figure 1 we can see the $(\Delta E_\gamma^x, \Delta E_\gamma^y)$ bitmap distribution of ^{171}Yb nucleus. Indeed, we can clearly observe the expected average grid of $8c \approx 71.0\ keV$ (green-colored) that corresponds to $\Im^{(2)}_{eff}$. However, we can also observe the emergence of an unexpected thinner equidistant grid at the distance of $2c \approx 17.8\ keV$ (brown-colored), or the quarter distance of the first grid. Both grids can be observed in the $2D$ distribution as well as in its $1D$ projection on the x axis.

Indeed, one can see that the points in the $(\Delta E_\gamma^x, \Delta E_\gamma^y)$ distribution *on average* tend to coalesce around both the $8c$ and $2c$ grids. Therefore, this distribution contains the unexpected thinner $2c$ *granularity* of the E_γ data besides the expected $8c$ one. We call this property of the $(\Delta E_\gamma^x, \Delta E_\gamma^y)$ data that *on average* coalesce to the double structure of $8c$ and $2c$ maxima *repeatability*.

To keep track of the newly found repeatability property, we can rewrite eq. 2 as:

$$E_\gamma(I) = 2c(2I + k - 1) \tag{4}$$

with k an integer number that accounts for the $2c$ thinner maxima. We can see that the $2c$ inertial parameter is a real number, while the $(2I + k - 1)$ angular momentum is an integer number. Thus, in eq. 4 we derived a new parametrization that describes *on average* both $8c$ and $2c$ granularities of the γ-ray energies.

2.2 Generalized ideal Bohr-Mottelson rotational bands

We can ask now: Is the property of repeatability general or depends on some particular conditions? We observed it in a number of even-A and odd-A nuclei, for normal deformed or superdeformed bands, which are very general conditions. However, for other nuclei the $2c$ grid is blurred by more intense fluctuations and can no longer be observed clearly.

To answer this question in Figure 2 we present the γ-ray energies versus spin of the rotational bands of ^{171}Yb nucleus. We can see that except for Bands 3 that deviate strongly from a straight line, all the others are almost linear and parallel, with relatively small deviations from a beam of parallel and equidistant lines. Indeed, if such a beam is fitted to the bands, it will capture the average behavior of the rotational bands of ^{171}Yb nucleus.

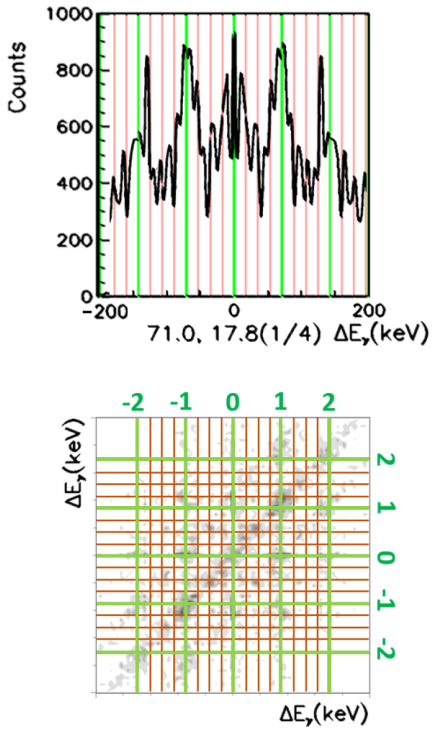

Figure 1. $(\Delta E_\gamma^x, \Delta E_\gamma^y)$ bitmap distribution of ^{171}Yb nucleus, with the $2D$ distribution in the lower part and the $1D$ projection on the x axis in the upper part. The $8c$ and $2c$ grids are drawn in green and brown colors, respectively. Unlike the *Fluctuation Analysis Method* mentioned in the text which uses experimental coincidence matrices with the well-known structure of ridges and valleys, here we use only the energy values for coincidences (therefore no coincidence peak intensities). The numbers on top and right-hand side of the $2D$ distribution indicate the relative positions of the coincidence ridges. Thus, the (I, J) crossing point collects coincidences form the I-th ridge on the x axis and the J-th ridge on the y axis relative to the minuend coincidence.

Therefore, to describe such a beam we need different offsets to the general dependence in eq. 2. We can do that by adding there a k integer number: $E_\gamma(I) = 2c(2I + k - 1)$. Doing so we can see that we got exactly the expression from eq. 4, which means that the *repeatability* we got from $(\Delta E_\gamma^x, \Delta E_\gamma^y)$ bitmap distribution in subsection 2.1 is equivalent with the *average* behavior of the rotational bands as a parallel and equidistant beam of straight lines.

Or, the dependence as the one in Figure 2 is quite general and characteristic for all high-spin rotational bands. Moreover, even the more deviating curves as Bands 3 are still increasing with spin and can be fitted with a straight ascending line for the average rotational behavior.

By that we get to a powerful conclusion: *Repeatability really is a ubiquitous property of high-spin data* which remained unnoticed or unnamed by now. Could this general property of E_γ data bring new physical insight into high-spin physics?

To answer this question let us determine the average $2c$ slope and the different k band offsets by a least-squares fit over all bands' γ rays. This can be done by minimizing the deviations from the straight lines of all the bands

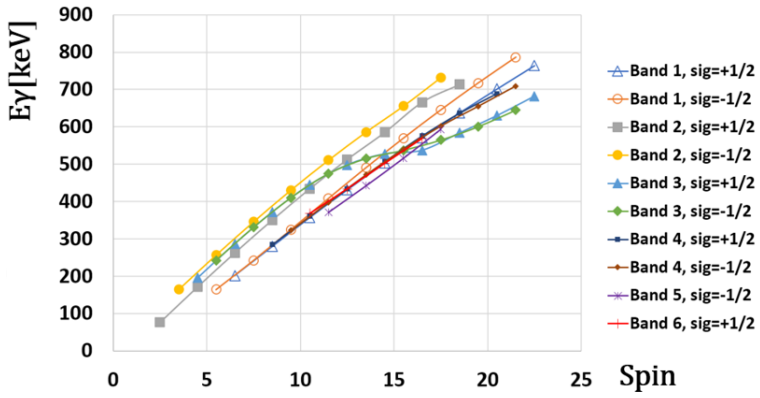

Figure 2. γ-ray energies (in keV) versus spin (in $\hbar$ units) of the rotational bands of ^{171}Yb nucleus [5].

simultaneously:

$$\sum (E_\gamma(I)/2c - (2I + k + 1))^2 = min \tag{5}$$

The k offset values obtained from fit for each of the fit lines are given in Figure 3. For the individual bands they are: $k = 6$ for Band 2 $sig = -1/2$, $k = 4$ for Band 2 $sig = +1/2$, $k = 2$ for Bands 3 (both signatures), $k = 1$ for Band 1 $sig = -1/2$, $k = 0$ for Band 1 $sig = +1/2$, Bands 4 (both signatures), and Band 6 $sig = +1/2$, and $k = -1$ for Band 5 $sig = -1/2$.

We also get the average slope $2c = 17.75keV$ from which we get the effective second moment of inertia that characterizes the average rotational motion of the ^{171}Yb nucleus:

$$\Im^{(2)}_{eff} = \frac{\hbar^2}{2c} = 56.34\,\hbar^2/MeV \tag{6}$$

Finally, in Figure 4 we present separately the beam of parallel fit lines from Figure 3. With the same constant effective second moment of inertia we call them *Generalized ideal Bohr-Mottelson rotational bands*: By repeatability they capture the average rotational behavior of ^{171}Yb nucleus.

Moreover, we can see how repeatability is indeed taken into account on the beam of parallel and equidistant lines. Thus, the difference between any two *intraband* γ rays is a multiple of $8c$, while the difference between any two *interband* γ rays is a multiple of $2c$.

Therefore, both $8c$ and $2c$ γ-ray granularities in the $(\Delta E^x_\gamma, \Delta E^y_\gamma)$ differential distributions from Figure 1 are also present in the beam of Generalized ideal Bohr-Mottelson rotational bands from the Figure 4. They both contain the same property: *Repeatability*.

3 Level scheme re-concept

In this section we present how the property of *Repeatability* of the E_γ data leads to the new concept of the *Double Helix Level Scheme*.

3.1 Effect of repeatability on level structure

In the previous section we got the generalized ideal Bohr-Mottelson rotational bands for the average description of ^{171}Yb bands. Regular level schemes are built from the ground state by adding up the energies of γ transitions. Is the new $2c$ granularity of the γ transitions going to affect the structure of levels scheme?

To answer this question, we first observe that for $k = 0$ the generalized ideal Bohr-Mottelson rotational bands are described by the $I(I + 1)$ rule. The corresponding level structure that we present in Figure 5 is that of a regular rotational band, shown for illustration for even and odd spins.

For $k \neq 0$, the generalized ideal Bohr-Mottelson rotational bands have the same moment of inertia, $\Im^{(2)}_{eff}$, (same $2c$ slope) but are no longer described by the $I(I + 1)$ rule. How to place the k-generalized ideal rotor bands in the levels scheme?

To answer this question, we take a different approach from the common "band by band" level scheme representation. The goal is to transfer the $2c$ granularity from γ rays to levels in a direct and compact way. Thus, this can be simply done by adding $2I + 1$ "stairs" of $2c$-equidistant levels to the $k = 0$ levels in Figure 5. In this way the $2c$ granularity of the γ rays is directly transferred to the level scheme structure.

The resultant pattern is the *open parabolic* $2D$ *structure* that we show in Figure 6. In fact, two separate ranges of stairs emerge, one for the even spins (in black) and other for the odd spins (in red).

Why having exactly $2I + 1$ stairs for each $I, k = 0$ level is because if we continue to add extra stairs on both sides of the ranges, then the stairs going down from the I range will match the energy of those going up from the level $I - 2$. Thus, for example, if we add the -7 and -8 steps to the left of the $I = 6$ range, they will match the energies of the 4 and 3 steps to the right of the $I = 4$ range. This will get a spurious degeneracy of the levels.

On the open parabolic $2D$ structure of Figure 6 the $k = 0$ bands are vertical paths, while the $k \neq 0$ ones are tilted paths: from right to left for the $k > 0$, and from the left to right for the $k < 0$, respectively. We can now see that repeatability is implemented in the level scheme by two different scales: $8c$ which gives the parabolic scale of the $k = 0$ levels; and the new $2c$ linear scale of the $k \neq 0$

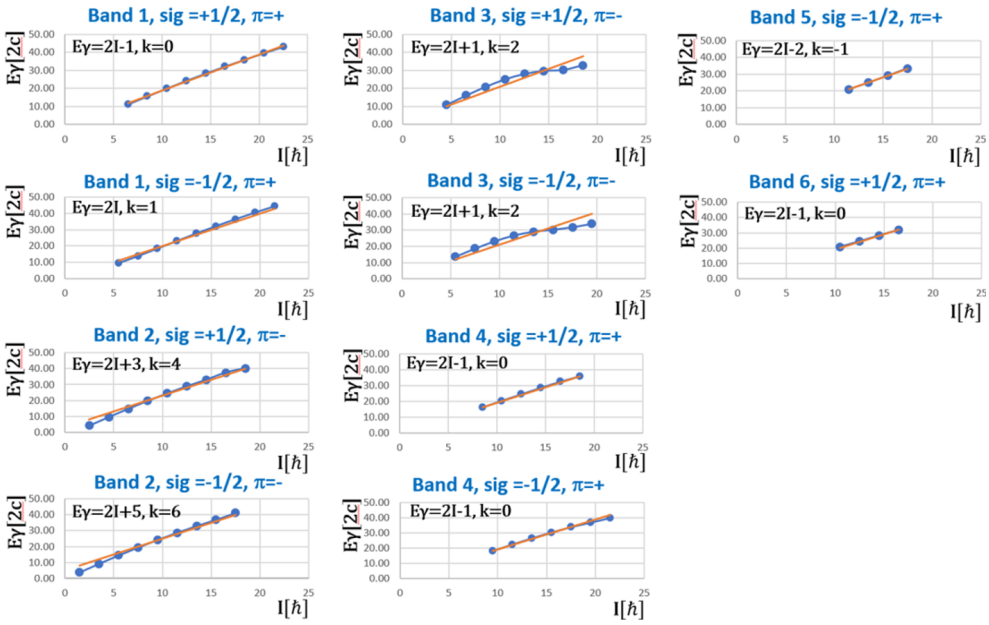

Figure 3. Least-squares fit of the γ-ray energies of the rotational bands of ^{171}Yb nucleus with the $2c(2I + k - 1)$ straight lines to determine the average slope $2c$ and the k values for the individual bands. The straight lines (in brown color) determined by fit are superposed on the experimental points of each band (in blue).

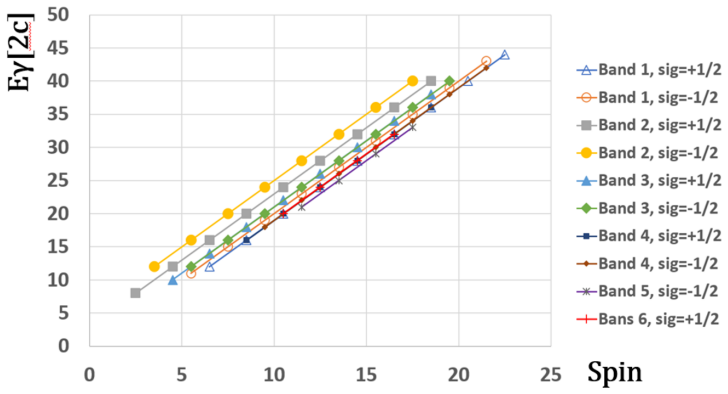

Figure 4. Generalized ideal Bohr-Mottelson rotational bands describing the average behavior of the experimental bands of the ^{171}Yb nucleus determined by the fit in Figure 3.

levels. In general, the energy levels can be indexed by three integer numbers, (I, m, E), where:
- I is the nuclear spin,
- m is the position of the "stair" level relative to the spin "floor",
- E is the energy of the level, which is a natural number in units of $2c$.

We can see that the (I, m, E) triplet of coordinates suggests $3D$ level scheme.

3.2 Parity for repeatability level structure

We should now endow the repeatability open $2D$ parabolic level structure with parity. For this purpose, we adopt the concept of reflection with respect to a mirror-like plane.

This is illustrated in Figure 7 where we postulate *positive parity* for the $2D$ structure on the right-hand side, for which the energy of the stairs-like levels increases to the right. Similarly, we postulate *negative parity* for its symmetrical structure with respect to the mirror-like plane on the left, for which the energy of the levels increases to the left. Same concept transfers to the derived helicoidal structures in the next sections.

3.3 Double helix for even-A and odd-A nuclei

How can the $3D$ prototype of the level scheme can be obtained from the open parabolic $2D$ structure? Intuitively, if we associate the $2D$ structure with fire escape stairs on a flat building facade and we reshape it as a parabolic

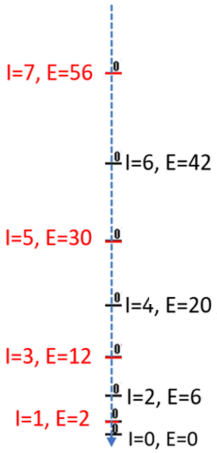

Figure 5. Level structure for generalized ideal Bohr-Mottelson rotational bands for $k = 0$ (in units of c) for both even and odd spins.

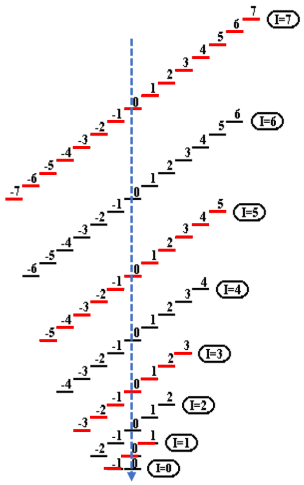

Figure 6. Level structure for generalized ideal Bohr-Mottelson rotational bands for $k \neq 0$ (in units of $2c$) for both even and odd spins added to that of the $k = 0$ bands from Figure 5.

tower, then the stairs will spiral down against the wall of the tower.

The two ranges of stairs, one for even spins and one for odd spins, transforms each into a helicoidal range. Therefore, through repeatability *double helix* becomes the prototype of rotational level scheme.

In Figure 8 we present the $3D$ double helix structure for even-A nuclei (viewed from above). We adopted the set with both helicoids rotating counterclockwise. However, we should keep in mind that the clockwise rotating double helix structure is equally possible, as well as the full set of four helicoids with both directions of rotation.

The direction of rotation degree of freedom that comes naturally with the new concept of double helix level

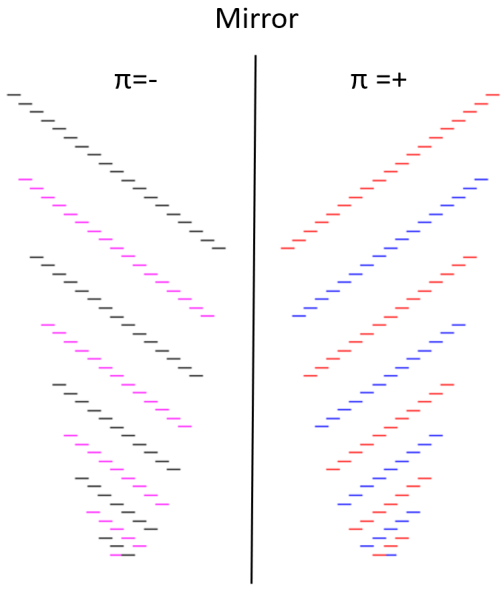

Figure 7. Illustration of parity concept by mirror-like reflection symmetry. By convention, if the energy of stairs-like levels increases to the right, the parity is positive (right part of the figure); otherwise, if stairs-like levels energy increases to the left, the parity is negative (left part of the figure). Same concept transfers to the derived helicoidal structures.

scheme is one of the potential benefits of our approach. As this stage it is unclear if nuclei would manifest one or another of the directions of rotation, or both.

If the rotation of the levels in the level scheme can be associated with the rotation of nuclear matter itself, then double helix will become a powerful tool to explore directly whether nuclear matter rotates to the left or to the right, or even in both directions for an individual nucleus.

Next, in the upper corners of Figure 8 we indicated the four possible combinations of signature-parity (sig, π) for the rotational bands. In the new double helix level scheme rotational bands are represented as decay paths superimposed on the double helix, which thus serves as a support or a skeleton for the real bands.

Thus, the bands corresponding to the two combinations of (sig, π) from the left-hand corner get represented on the blue helicoid, while those corresponding to the two combinations of (sig, π) from the right-hand corner get represented on the magenta helicoid.

Finally, in Figure 9 we present the similar structure of counterclockwise double helix for the half-integer spins of odd-A nuclei, on which we are going to superimpose the rotational bands of ^{171}Yb nucleus. In analogy with the even-A case, the two combinations of (sig, π) from the left-hand corner get represented on the blue helicoid, while those corresponding to the two combinations of (sig, π) from the right-hand corner get represented on the cyan helicoid.

As I is total angular momentum, it results that $(2I + k - 1)$ expression is the *generalized angular momentum* of the generalized ideal Bohr-Mottelson rotational bands; hence

k has the dimension of angular momentum as well. This gives $\hbar$ as unit for the axes in Figures 8 and 9.

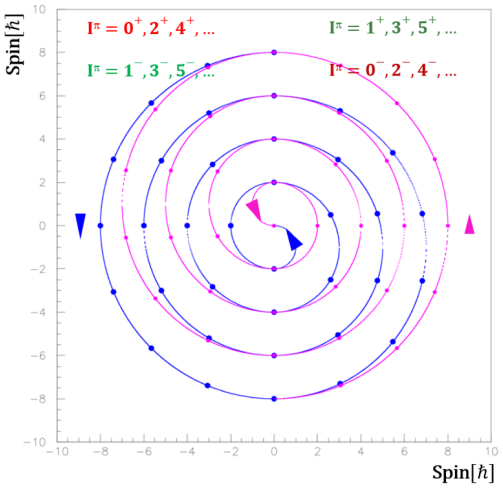

Figure 8. Double helix with counterclockwise rotation for integer spins of even-A nuclei. Bands of spin-parity combinations from the upper left corner of the figure are represented on the blue helicoid, while those of the spin-parity combinations from the upper right corner of the figure are represented on the magenta helicoid.

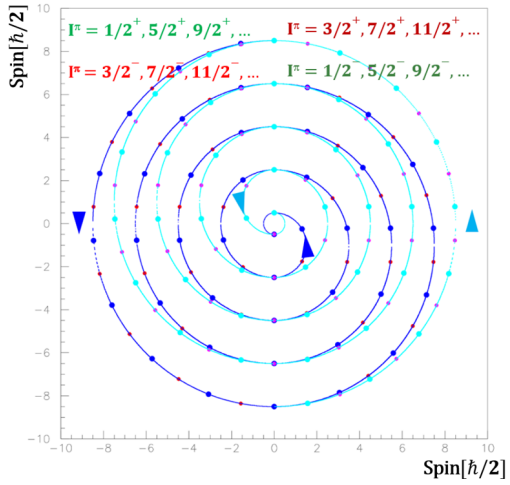

Figure 9. Double helix with counterclockwise rotation for integer spins of odd-A nuclei. Bands of spin-parity combinations from the upper left corner of the figure are represented on the blue helicoid, while those of the spin-parity combinations from the upper right corner of the figure are represented on the cyan helicoid.

3.4 Level scheme of generalized ideal Bohr-Mottelson rotational bands

We are now able to show how the $(2I + k - 1)$ generalized ideal Bohr-Mottelson rotational bands from Figure 4 look when superimposed on the double helix. As at this stage we did not study the linking transitions by which they could be drawn as excited bands, we give a generic representation of a ground state band represented on the corresponding helicoid for different k values, for $k = 0 \pm 1$, ± 2, ± 3, ± 4, ± 5, ± 6, ± 7. The results are plotted in Figure 10.

As we can see most clearly in Figure 10 *(b)*, the bands tend to align to one of the x or y axes, with the even k values to the x axis and the odd k values to the y axis. For example, $k = 0$ band aligns along the positive y axis, $k = 1$ band along the positive x axis, $k = 2$ band along the negative y axis, and $k = 3$ band along the negative x axis, with the next four higher k values repeating the alignment for the first four ones. Same behavior is observed for the negative k values, but with the bands rotating counterclockwise.

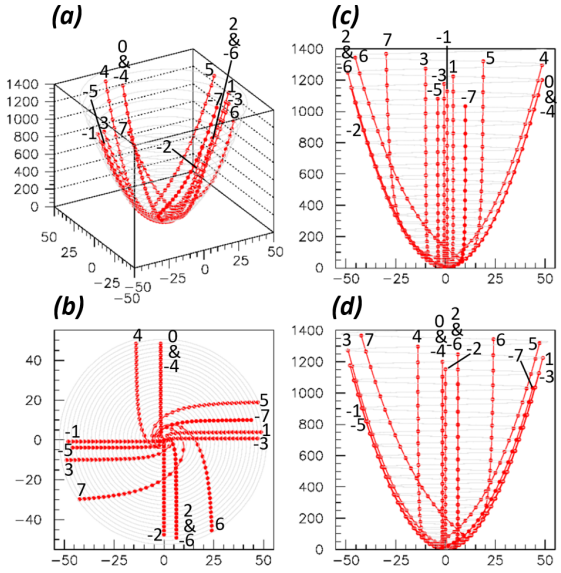

Figure 10. Generalized $(2I + k - 1)$ bands on helix for odd A nuclei. *(a)* 3D view; *(b)* 2D $x - y$ projection (view from above) ; *(c)* 2D $y - z$ projection (view from the right lateral face); *(d)* 2D $x - z$ projection (view from the front face).

3.5 Decomposition of experimental E_γ values

Let us now refer to the experimental E_γ values in Figure 3 and decompose them as the sum of the corresponding value on the fit line, plus the deviation of the experimental point from the fit line. Thus, we have:

$$E_\gamma(I) = 2c(2I + k - 1 + k' + fn) \tag{7}$$

with $2c(2I + k - 1)$ the fit value and $2c(k' + fn)$ the deviation. Next, we will refactorize this expression into the canonical real inertial parameter factor and integer angular momentum factor:

$$E_\gamma(I) = 2c_{band}(2I + k + k' - 1) \tag{8}$$

with the new *band inertial parameter* defined as:

$$2c_{band} = 2c[1 + fn/(2I + k + k' - 1)] \tag{9}$$

with the redefined $2c_{band}$ now varying with transition.

We can now calculate the *band second moment of inertia* defined as:

$$\Im^{(2)}_{band} = \frac{\hbar^2}{2c_{band}} \tag{10}$$

In Figure 11 we plot the values of $\Im^{(2)}_{band}$, which are oscillating functions of the nuclear spin I. We also drew the constant value of $\Im^{(2)}_{eff}$ corresponding to the average rotational motion of ^{171}Yb nucleus.

Eq. 8 gives the *complete repeatability description* of the experimental bands. It is an extension of the $2c(2I + k - 1)$ parametrization for the average rotational behavior from eq. 4 obtained in subsection 2.1.

3.6 Double helix level scheme of experimental rotational bands

With the decomposition from eq.8 we can proceed to represent the experimental bands decay paths on the double helix. The detailed procedure is described in [4]. Here we give only a brief review of it.

First, we need to get the band heads of the excited rotational bands, obtained from their linking transitions to the ground state Bands 2, or between one another. These are treated differently for the two groups of bands, the low excited group of Bands 1 and 3 and the high excited group of Bands 4, 5 and 6. If we use the typical decomposition of eq. 8[1], for the bands of the second group we get abnormally high placements on the double helix.

What is that? For an energy level of spin I, there is a whole energy interval covered by its $(2I+1)$ m states where this level is expected to be located on the double helix. Or, while the bands in first group satisfy this rule, those in the second group get placed in the range corresponding to the next $I+2$ level, an abnormal *overscaling* effect. As remedy, these bands were applied an operation of *rescaling* that brought them back into their normal ranges.

Secondly, due to repeatability we get two different scales to represent on the double helix: the level energies as for the common level schemes, and the generalized angular momentum. For each level we place first its generalized angular momentum, which is an integer number matching one of the double helix points; then by a real-number interpolation method we alter it to match its level energy value.

Thus, we get a final unique position of the levels on the double helix with satisfying both energy and generalized angular momentum conservation laws. Finally, for each band we connect the levels thus placed with curved lines of the same color as the levels, which indicate the γ transitions.

The resulting double helix level scheme of ^{171}Yb nucleus is given in Figure 12. Only the in-band $E2$ transitions are represented. For clarity no linking or $M1$ crossover transitions were drawn. For the same reason we also omitted the arrow heads for transitions.

[1]Linking transitions are either of the $E2$ multipolarity, in which case we use eq. 8; or $M1$, in which case we use the decomposition $E_\gamma(I) = 2c_{band}(I + k + k')$ obtained similarly for this multipolarity.

As we observe in the figure, unlike Figure 10 where to consecutive γ transitions correspond complete 2π rotations of the helicoid, the experimental bands do no longer align to the x or y axis directions, but precess on the helix giving their characteristic clockwise or counterclockwise apparent rotations on the helicoids. Moreover, half of the bands manifest the *backbending* phenomenon.

In concluding this section, let us observe that while the energy scale is the same as for the regular level schemes, the new generalized angular momentum scale added by repeatability gives not only the paraboloid of the $3D$ level scheme, but also transforms the bands into precessing paths on the double helix.

4 Physical insight into high-spin physics

In this section we attempt a more systematic view at the ^{171}Yb double helix level scheme and what it can bring new to the big picture of high-spin physics.

4.1 Elementary helix loop with γ transition

Common level schemes are done by repeating the elementary pattern of initial and final levels interconnected by the decaying γ transition along each rotational band.

For the double helix level scheme, the initial and final levels are not only connected by the γ transition, but also by the elementary helix loop. Based on Figures 10 and 12, we get two types of such loops.

To characterize the loop, we first define the *phase angle* for any level of the double helix:

$$\theta(I, m) = \sum_{(I,m)} (I + \frac{m}{I})\pi \tag{11}$$

Then, the *phase shift* between the levels of an elementary loop are defined by:

$$\Delta\theta(I) = \theta(I) - \theta(I - 2) - 2\pi \tag{12}$$

In Figure 13 we present the typical elementary loops:

(a) The $\Delta\theta = 0$ loop is characteristic for the full 2π *macroscopic rotation* of the $(2I + k - 1)$ bands from Figure 10. For such bands k is fixed, therefore for each loop the 2π rotations are systematically produced only by the $2I$ component. The effective moment of inertia $\Im^{(2)}_{eff}$ is constant that implies no contribution of the intrinsic microscopic motion, which supports the argument that this corresponds to the pure macroscopic rotation of the whole nucleus. The specific γ-decay paths are along the x and y axis.

(b) The $\Delta\theta \neq 0$ phase shifts are due to the cumulated $(k + k')$ effects of the *microscopic intrinsic motion* on the $2I$ macroscopic motion in the $(2I + k + k' - 1)$ bands. This produces the specific apparent rotations (precessions) of the decay paths on the double helix in Figure 12.

Thus, for $\Delta\theta(I) < 0$ ($\Delta\theta(I) > 0$) the microscopic rotation itself should be clockwise (counterclockwise) to give the corresponding clockwise (counterclockwise) precessions of the γ-ray decay paths.

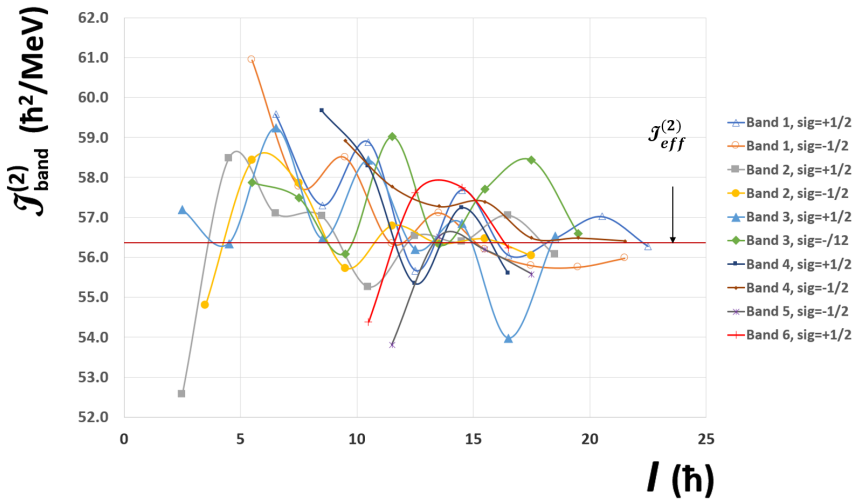

Figure 11. Band second moment of inertia $\mathfrak{I}^{(2)}_{band}$ as defined in the text for the bands of ^{171}Yb nucleus shown on the right.

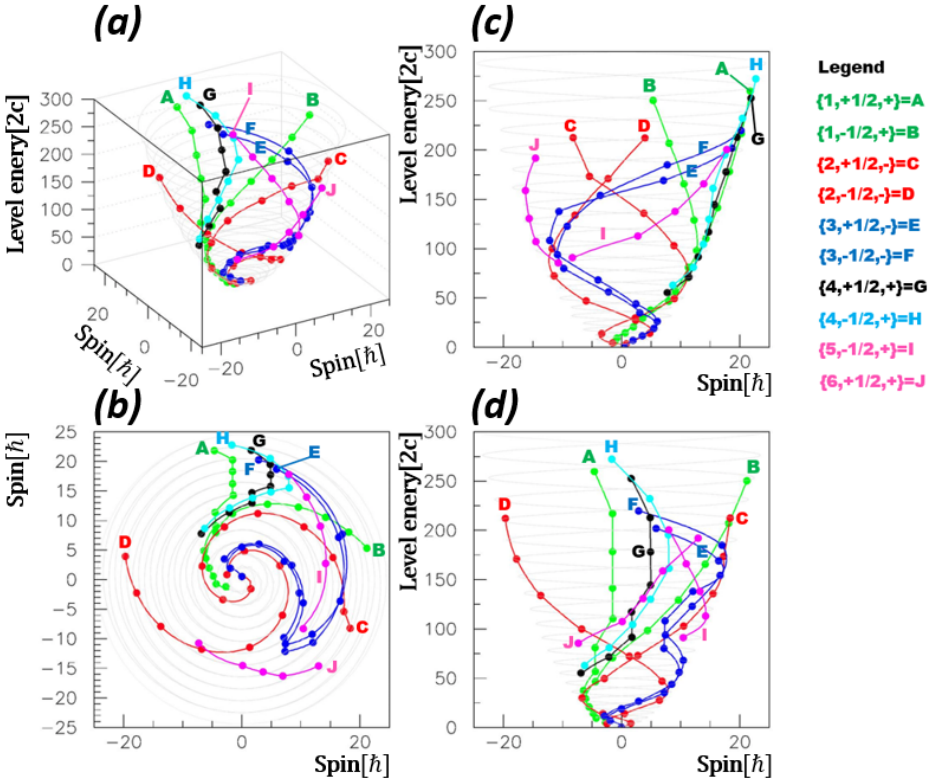

Figure 12. Double helix level scheme of ^{171}Yb nucleus for the bands from [5] as shown in the legend on the right. The four panels are defined in Figure 10. On the right-hand side legend we show in braces the band number, signature, and parity for each band.

Therefore, the $(2I + k + k' - 1)$ parametrization specific to the double helix level scheme responds in a similar way as the macroscopic-microscopic method on the basic approach of the liquid drop model [8]. This can give a first insight on how the double helix responds to high spin physics.

In fact, each of the three components of the $(2I+k+k'-1)$ parametrization play a specific role. First, the $2I$ component gives the straight-down rotational bands accompanied by the overall 2π macroscopic rotation of the helix loops. Then, the k component moves the straight-down bands in the four $\pi/2$ directions in Figure 10, keeping the 2π rotation of the helix loops. Ultimately, it is only the k' component that gives the precessions of the bands on the double helix, to say so the purely microscopic component.

Thus, if in the traditional macroscopic-microscopic picture the two terms are intermingled by the Strutinsky shell correction applied to the deformed liquid drop [8],

now we get the k explicit contribution intermingling between the $2I$ and k' extremes, which would correspond to a *macroscopic-mesoscopic-microscopic* picture of three sub-scales of the nuclear motion. When studied properly, this can give a new insight in high-spin physics as well.

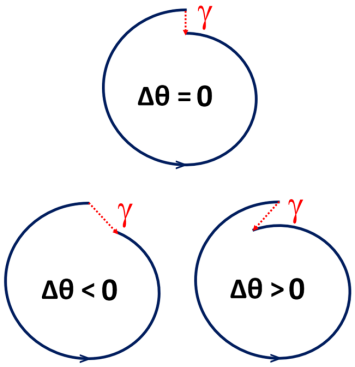

Figure 13. Elementary phase shifts as defined in eq. 12 for the $E2$, $\Delta I = 2$ γ transitions shown as red arrows between the open extremities of elementary helix loops.
Upper part: $\Delta\theta = 0$ phase shifts corresponding to the 2π helix loop characteristic to the $(2I + k - 1)$ bands in Figure 10.
Lower part: $\Delta\theta \neq 0$ phase shifts due to the cumulative $(k + k')$ effects coming from the interference of the microscopic intrinsic motion on the $2I$ macroscopic one in the $(2I + k + k' - 1)$ bands, giving apparent rotations (precessions) of the decay paths on the double helix, as seen in Figure 12. For $\Delta\theta(I) < 0$ ($\Delta\theta(I) > 0$) the microscopic rotation itself is clockwise (counterclockwise), giving the corresponding clockwise (counterclockwise) precessions of the γ-ray decay paths on the double helix.

4.2 Clockwise to counterclockwise phase transition

In Figure 14 we collected all the values of the $\Delta\theta$ phase shifts extracted for ^{171}Yb nucleus. We can see that at high spins and high excitation energies most of the bands experience the clockwise intrinsic rotation regime, while for the low spins and excitation energies they turn to the counterclockwise intrinsic rotation regime.

These two regimes can be associated with two phases of the intrinsic motion. When the bands cross the $\Delta\theta = 0$ borderline a phase transition takes place, which in Figure 12 *(b)* takes the form of the *backbending* phenomenon. Moreover, if the crossing of the $\Delta\theta = 0$ borderline is sharp, the corresponding backbending is also sharp. On the contrary, if the bands align a number of points along $\Delta\theta = 0$ axis, then the backbending is more gradual.

Thus, we can observe that Bands 5 and 6 stay only in the clockwise regime, while Bands 2 and Band 1 $sig = -1/2$ only in the counterclockwise one; therefore, they do not change the direction of rotation. However, all the other five bands do change their apparent direction of rotation and consequently manifest backbending in Figure 12 *(b)*.

Thus, Bands 3 which cross the $\Delta\theta = 0$ borderline sharply get a very sharp backbending. The remaining Bands 4 and Band 1 $sig = +1/2$ start with the clockwise regime at high excitation energies and spins, but then turn to the counterclockwise regime at lower excitation energies and spins. Each aligns in order 2, 3 and 4 levels to the positive direction of the y axis, which makes their backbending less and less sharp.

In the lower excitation energies and spins region, all bands coalesce toward the opposite arms of Bands 2, the ground state bands. Thus, Bands 3 coalesce toward Band 2 $sig = -1/2$, while Bands 1 and 4 toward Band 2 $sig = +1/2$, together with which they precess orderly in the counterclockwise direction to the ground state.

5 Conclusions

We can now understand better what the double helix really is. It resulted unexpectedly from the ubiquitous *repeatability* property of the experimental E_γ data that made the breakthrough to the double helix level structure.

The $(\Delta E^x_\gamma, \Delta E^y_\gamma)$ differential distributions from Figure 1 that revealed the hidden $2c$ granularity of the E_γ data are equivalent with the well-known E_γ *vs Spin* dependencies from Figure 2. Altogether they gave the $E_\gamma = 2c(2I+k-1)$ parametrization with I, k integers, by which we transposed repeatability into the double helix structure of the levels.

The k angular momentum transforms into the m integer number in the (I, m, E) triplet of double helix levels, with values ranging from $-I$ to I. Therefore m can be identified with the projection quantum number of the total angular momentum I on the z axis.

It transfers repeatability from the γ data to the $I(I + 1)$ quadratic level structure, on which the experimental bands described by the $2c_{band}(2I + k + k' - 1)$ parametrization from eq. 8 are superimposed as decay paths. To some extent, double helix can be seen as the underlying structure of high-spin nuclear structure itself.

Double helix is the geometrical locus of the (I, m, E) rotational states the nucleus as a whole can use for nuclear rotation, which defines a *meta-trajectory* of level energies E as function of generalized angular momentum, (I, m).

One cannot know if quantum mechanically the rotating nucleus passes through all these states; instead, the double helix structure is probed by the real rotational bands swirling down the double helix structure. Semiclasically, it is like *on average nuclear matter itself follows the meta-trajectory of the double helix*, with the actual levels selected by the rotational bands' paths.

Double helix is not a direct description of the rotating nucleus quantum reality, but just another semiclassical model of nuclear rotation deduced from our interpretation of the experimental data. Similarly, the well-studied deformed liquid drop model is a semiclassical model of quantum reality.

Semiclassically, through repeatability nuclear matter's double helix motion can be seen as a *vortex motion*. It preserves the quantum attributes of the nuclear motion as signature - one for each helicoid - and parity, as well as the backbending phenomenon associated in this model with changing the direction of intrinsic motion from clockwise to counterclockwise.

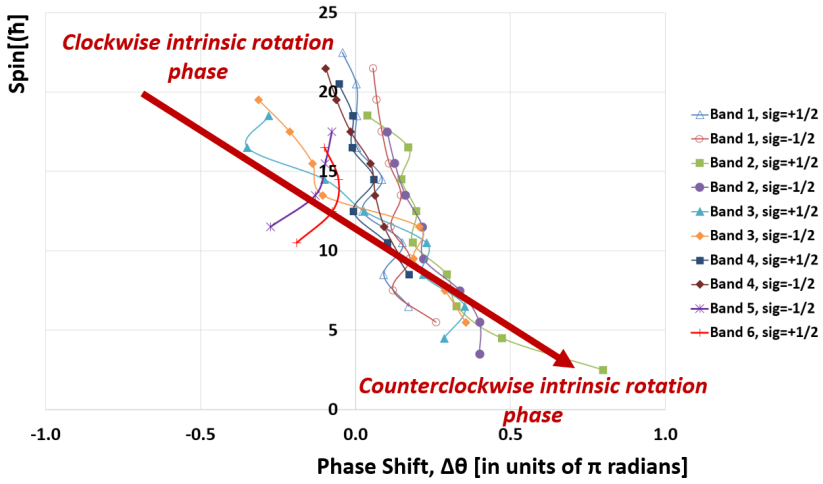

Figure 14. Phase shifts $\Delta\theta$ values extracted for ^{171}Yb nucleus

Overall, double helix can indicate vorticity in the liquid drop and relax the irrotational flow hypothesis on Bohr-Mottelson model. It can presumably be integrated as a vortex into the liquid drop, or further developed independently.

Vortex is the admixture mechanism at the contact of two media, as cold or hot air, dry or humid, of higher or lower pressure in tornados or hurricanes. It is par excellence a very efficient natural dissipation mechanism of angular momentum and energy. It would be no surprise that it can serve the same purpose even for the nuclear rotor, which results from the admixture of the two media of target and projectile nuclei as well.

There is one case scenario when the double helix model could be effective: spontaneous nuclear fission. Thus, the classical dynamics of fission starts with the gradual elongation of the liquid drop-modelled nucleus, which develops a neck which finally breaks. The kinetic energy corresponds to the translation of the fragments after fission. But how the fragments get the large amounts of angular momentum needed for the high-spin states populated in the process?

Indeed, there are many high spins studies based on fission fragments, for example from the spontaneous fission of ^{248}Cm and ^{252}Cf nuclei when the fragments get the large amounts of angular momentum. However, simple elongation alone seems insufficient to provide the required amount of angular momentum.

Instead, we can suppose that a latent double helix structure is folded in the ground state of the spheroidal fissioning nucleus. When deformation begins, the double helix structure unfolds and transfers the two yet unseparated fragments, with a double helix for each fragment rotating in opposite directions on each side of the neck.

Thus, during the elongation process the two fragments accumulate large amounts of angular momentum of opposite orientations as well as excitation energy, which after scission get dissipated through the γ-ray cascades by the now freed double helices. Fission can thus become a test ground for the double helix model of nuclear rotation.

References

[1] A. Bohr, B.R. Mottelson. *Nuclear Structure*, vol. 2, (W.A. Benjamin, New York (1975))

[2] WU Xi, LEI Yi-An, Chin. Phys. C **Vol. 32**, No. 2, 112 (2008). https://doi.org/10.1088/1674-1137/32/2/008

[3] D. Bucurescu, N. Marginean, Phys. Rev. Lett. **79**, 31 (1997). https://doi.org/10.1103/PhysRevLett.79.31

[4] N. Nica, *Double Helix Level Scheme of ^{171}Yb Nucleus*, accepted at At. Data Nucl. Data Tables.

[5] D.E. Archer et al., Phys. Rev. C **57**, 2924 (1998). https://doi.org/10.1103/PhysRevC.57.2924

[6] B. Herskind et al., Phys Lett B **276**, 4 (1992). https://doi.org/10.1016/0370-2693(92)90533-A

[7] B. Herskind et al., Phys Rev Lett **68**, 3008 (1992). https://doi.org/10.1103/PhysRevLett.68.3008

[8] P. Möller, A.J. Sierk, Int. J. Mass Spectrom. **349–350**, 19 (2013). http://dx.doi.org/10.1016/j.ijms.2013.04.008